Flux-Weakening Control of Dual Three-Phase PMSM Based on Vector Space Decomposition Control

Yashan Hu, Yonggang Li, Xiandong Ma, Xuefei Li, and Shoudao Huang, *Senior Member, IEEE*

***Abstract*—This article proposes a flux-weakening (FW) control for dual three-phase permanent magnet synchronous machine (DT-PMSM) based on vector space decomposition (VSD) control, where the output voltage in $\alpha\beta$ subplane is employed for voltage feedback in the FW control loop. As the fundamental components are mapped to $\alpha\beta$ subplane while the fifth and seventh harmonics are projected to harmonic z_1z_2 subplane, the FW current from this new control in $\alpha\beta$ subplane is sixth harmonic-free regardless of the fifth and sixth harmonics being resulted from the nonsinusoidal back electromotive force (EMF) or inverter nonlinearity. The proposed control is compared with the conventional FW feedback control extended for DT-PMSM, where the FW control is applied to the two sets of three-phase windings separately. The experimental results show that the proposed FW control based on VSD is superior to the conventional FW control in terms of reduction in current unbalance and harmonic currents.**

***Index Terms*—Double star permanent magnet (PM) machine, dual three-phase PM synchronous machine (SM), flux-weakening (FW) control, six-phase pm machine, vector space decomposition (VSD).**

NOMENCLATURE

F_α, F_β	Components in the $\alpha\beta$ subplane.
F	Can be R, v, i, ψ_s or ψ_f, which represents stator resistance, voltage, current, stator flux-linkage, or PM flux-linkage.
F_{z1}, F_{z2}	Components in the z_1z_2 subplane.
$\boldsymbol{F}_{\alpha\beta}$	Vector $F_\alpha + j\,F_\beta$.
$\boldsymbol{F}_{\boldsymbol{z1z2}}$	Vector $F_{z1} + j\,F_{z2}$.
$F_{\alpha 1}$, $F_{\beta 1}$	Components of phase-ABC in $\alpha\beta$-frame.
$F_{\alpha 2}$, $F_{\beta 2}$	Components of phase-XYZ in $\alpha\beta$-frame.
$\boldsymbol{F}_{\alpha\beta 1}$	Vector $F_{\alpha 1} + j\,F_{\beta 1}$.
$\boldsymbol{F}_{\alpha\beta 2}$	Vector $F_{\alpha 2} + j\,F_{\beta 2}$.
F_d, F_q	Components in dq-frame in $\alpha\beta$ subplane for DT-PMSM.
F_{dz}, F_{qz}	Components in dqz-frame in z_1z_2 subplane for DT-PMSM.
F_{d1}, F_{q1}	Components in the dq-frame for phase-ABC.
F_{d2}, F_{q2}	Components in the dq-frame for phase-XYZ.
$v^*_{\max}$	Voltage magnitude reference.
v_m	Voltage magnitude feedback in $\alpha\beta$ subplane.
v_{m1}	Voltage magnitude feedback for phase-ABC.
v_{m2}	Voltage magnitude feedback for phase-XYZ.
θ_e	Rotor electrical angle.
ω_e	Electrical speed.

Manuscript received August 10, 2020; revised October 19, 2020; accepted November 28, 2020. Date of publication December 14, 2020; date of current version March 5, 2021. This work was supported in part by the Huxiang High-Level Talent Gathering Project of Hunan Province under Grant 2019RS1013, in part by the Natural Science Foundation of Hunan Province under Grant 2020JJ4006, and in part by the Key Research and Development Project of Changsha, Hunan Province, China under Grant KQ2004019. Recommended for publication by Associate Editor U. Deshpande. *(Corresponding author: Yashan Hu.)*

Yashan Hu, Yonggang Li, Xuefei Li, and Shoudao Huang are with the College of Electrical and Information Engineering, Hunan University, Hunan 410000, China (e-mail: hu_ya shan@sina.com; 854354553@qq.com; fancy0xue@hotmail.com; 11097846@qq.com).

Xiandong Ma is with the Engineering Department, Lancaster University, Lancaster LA1 4YW, U.K. (e-mail: xiandong.ma@lancaster.ac.uk).

Color versions of one or more figures in this article are available at https://doi.org/10.1109/TPEL.2020.3044574.

Digital Object Identifier 10.1109/TPEL.2020.3044574

I. INTRODUCTION

SINGLE three-phase inverter-fed machine has been extensively used in various industrial applications. However, the inverter rating is difficult to increase up to a certain level due to the limitation on the power rating of semiconductor devices. Two attractive solutions to this problem are either using multilevel inverter or multiphase machines. Whether it is better to use multiphase machines or multilevel converters depends on the application. The insulation level is one of the limiting factors that hinder the use of the multilevel inverter. Therefore, the multiphase inverter-fed machines operating at a lower voltage level are preferred [1].

Compared with the single three-phase counterpart with the same drive current limit, the multiphase machine offers many advantages such as multiple power capacity, reduced torque pulsation, reduced stator current, lower dc-link current harmonics, higher reliability at the system level, increased power density for the same volume machine, and additional degrees of freedom, and can be driven by multiple single three-phase inverters [2]–[9]. The dual three-phase permanent magnet synchronous machine (DT-PMSM) has double power capacity and the characteristic of sixth-order torque harmonic pulsation-free. Over the last decades, it has been widely applied to many industrial applications such as aerospace, electric vehicles, "more-electric" aircraft, and wind turbines [8], [10]–[13].

The power topology of a dual three-phase voltage source inverter (VSI) drive, i.e., dual inverter, can be illustrated in Fig. 1, which is constructed by two single three-phase H-bridge VSIs with a common dc voltage source [7]. The asymmetrical DT-PMSM has two sets of single three-phase windings, where the first set is named as phase-ABC, whilst the second set is named as phase-XYZ. The electrical phase shift angle between phase-ABC and -XYZ is 30°, which is determined by the relationship of the measured phase back electromotive force (EMF),

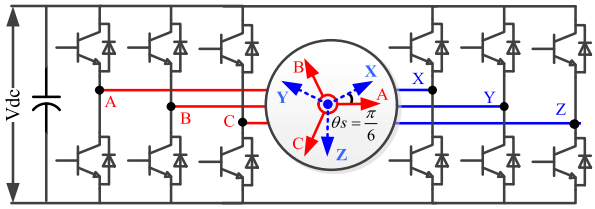

Fig. 1. DT-PMSM drive system.

and the neutral points for phase-ABC and -XYZ are isolated. A dual inverter is used to drive phase-ABC and phase-XYZ. When the DT-PMSM works under a regenerative braking mode, the dual inverter works as a boost rectifier and transfers power from DT-PMSM to the dc bus.

To extend the power and speed operation range, which is constrained by a given dc-link voltage, the flux-weakening (FW) control is usually adopted to weaken the air-gap flux by utilization of the FW current (*d*-axis current) [14]–[16]. Based on the conventional decoupling vector control with *dq*-axis current regulation for a single three-phase machine, the strategies of FW control can be classified into feedforward [17]–[22] and feedback methods [16], [23]–[32]. The FW control of the feedforward method has the advantage of excellent dynamic performance; however, the accuracy of FW current from the feedforward method relies heavily on the accuracy of machine parameters, such as the flux-linkage and inductances, which might vary with loads and temperature [18], [33], [34]. The feedback method is robust against the deviation of machine parameters; however, its dynamic performance is not as good as the feedforward method. To solve this issue, the feedforward and feedback methods can be combined in a hybrid method [35], [36].

The feedback in the FW control of the feedback method can be the voltage magnitude error [16], [24]–[28], the voltage error before and after the pulsewidth modulation (PWM) module [31], [32], or the error between the PWM period and the calculated active time for the synthesis of voltage vector command [37]. The first method is applicable under both linear PWM and overmodulation regions due to alterable voltage reference; however, the latter two methods are specifically designed for the overmodulation region and, thus, cannot achieve a FW operation in the linear PWM region. Although the FW operation in the overmodulation region can increase the power capability, it also results in increased harmonic voltage, current, and torque ripple, which might not be applicable in some applications demanding small torque ripples such as the MW wind turbine PMSM generator.

In terms of the vector control of DT-PMSM, it can generally be divided into two categories [38]. The first is two-individual current control, which is based on the double *dq* synchronous frames (d_1q_1-d_2q_2-frame) model with mutual coupling voltages between two frames, i.e., d_1q_1-frame for the first set of three-phase windings (phase-ABC) and d_2q_2-frame for the second three-phase windings (phase-XYZ) [6], [7], [39], [40]. If neglecting compensation of the mutual coupling between phase-ABC and -XYZ, two commercial single three-phase drives can work separately to drive the DT-PMSM with the equal torque command.

The second vector control strategy of DT-PMSM is the vector space decomposition (VSD) control [3], [41] with two current regulators in the $\alpha\beta$ subplane and two current regulators in the z_1z_2 subplane. The VSD control is prevailing as the DT-PMSM can be treated as a single three-phase machine in the $\alpha\beta$ subplane and a resistance inductance (*RL*) load in the z_1z_2 subplane. since there is no mutual coupling between the $\alpha\beta$ subplane and z_1z_2 subplane [3], [42], therefore, it can provide an excellent dynamic torque performance.

Theoretically, the FW control of DT-PMSM can be implemented based on the aforementioned two-individual current control and VSD control. The efficiency of dual inverter drives for the series split symmetrical DT-PMSM considering the field weakening region is discussed in [43], where the phase shift angle between two sets of three-phase windings is zero. In [43], the machine is treated as two separate single three-phase machines, and two independent drivers with their corresponding FW control are adopted.

The concept of FW control based on direct torque control (DTC) for a DT-PMSM is presented in [44], the DT-PMSM is treated as a six-phase machine based on the VSD theory [3], and the voltage and current in $\alpha\beta$ subplane are employed for the flux-linkage feedback. However, the harmonic components in the z_1z_2 subplane are not considered. As there might be abundant fifth and seventh harmonic voltages, resulted from inverter's nonlinearity and machine's nonsinusoidal back-EMF, it will result in abundant fifth and seventh harmonic currents if without current regulation in z_1z_2 subplane [41]. Meanwhile, the experimental results are not provided for validation. A FW control based on VSD control is presented in [45], where the FW is activated simply by the speed. When the speed is lower than the switching speed, it works under the $i_d = 0$ control, while when the speed is higher than the switching speed, it switch's to FW control with *d*-axis voltage command output directly without FW current control anymore.

In DT-PMSM, individual *dq*-axis voltages in the d_1q_1-d_2q_2-frame contain the sixth harmonic component. The sixth harmonic component will then propagate through the control loop and affect the harmonic content of the *d*-axis current. This article proposes a FW control based on VSD vector control to overcome this problem. With this new controller, the FW current from this new control is the sixth harmonic free regardless of the fifth and seventh harmonics resulted from the nonsinusoidal back-EMF and inverter nonlinearity. First, the conventional FW feedback control extended for asymmetrical DT-PMSM is studied, where the conventional vector control and FW control for a single three-phase system are applied to phase-ABC and -XYZ separately. The main deficiencies of the FW control based on two-individual current control will be discussed in detail in Section II, and then the reduction of current harmonics and unbalance of the proposed control is demonstrated in Section III. Finally, the comparative experiments are made on a prototype DT-PMSM, which validates that the proposed FW control is superior to the conventional FW control.

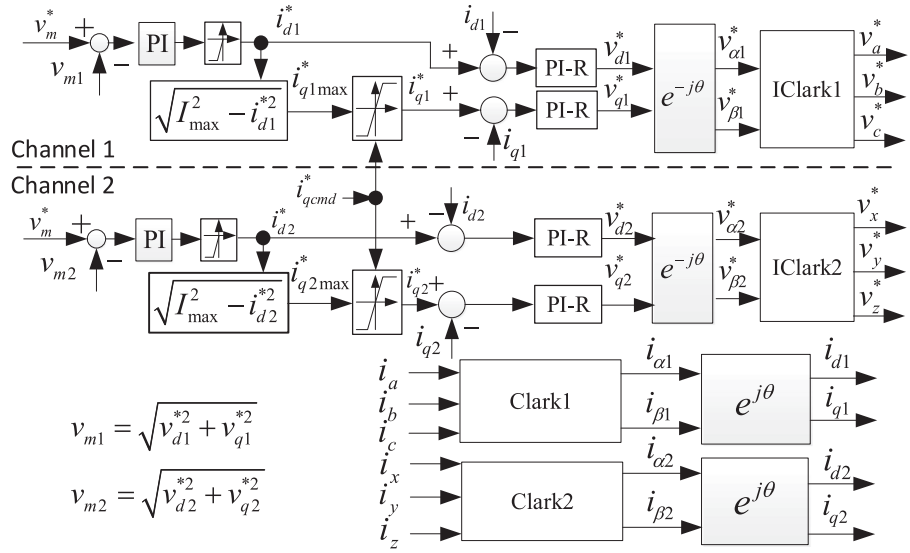

Fig. 2. Conventional FW control extended for DT-PMSM.

II. Conventional FW Control for Dual Three-Phase PMSM

The mathematical modeling of DT-PMSM based on the double synchronous dq-frames (d_1q_1-d_2q_2-frame) is detailed in [38]. If neglecting the mutual coupling voltages between phase-ABC and -XYZ, the DT-PMSM can be treated as two, single three-phase machines with coupling voltages between two sets of three-phase windings. Then the conventional FW control based on the voltage magnitude feedback for single three-phase PMSM [16], [24]–[28], [46] can be extended for DT-PMSM, which is demonstrated in Fig. 2. The FW control is based on the two-individual current control [7], [38], where two channels of the individual vector controller and FW controller are applied to each single three-phase windings. The upper and lower channels in Fig. 2 are for the control of phase-ABC and phase-XYZ, respectively. Both channels share the same quadrature current reference i_q^*, which might be from the speed control loop in the constant speed mode or torque control loop in the constant torque mode. The output voltage magnitude v_{m1} from phase-ABC in the first channel is employed for FW control of phase-ABC, while the output voltage magnitude v_{m2} from phase-XYZ is employed for FW control of phase-XYZ.

The FW current i_{d1}^* for phase-ABC and i_{d2}^* for phase-XYZ are then derived by the proportional-integral (PI) regulators with voltage error input. As the magnitude of current vectors is limited by the maximum current $I_{\max}$, the real quadrature current reference i_{q1}^* is the minimum value of i_q^* and $i_{q1\max}^*$ if i_q^* is positive, or the maximum value of i_q^* and $-i_{q1\max}^*$ if i_q^* is negative. This constraint is also applied to i_{q2}^* generation.

For a given dc bus volage $v_{\rm dc}$, the maximum linear output voltage with the space vector PWM (SVPWM) strategy is $v_{\rm dc}/\sqrt{3}$. Since the reserved voltage margin v_Δ accounting for the harmonic voltage is essential, consequently, the maximum output voltage magnitude v_m^* will be $v_{\rm dc}/\sqrt{3}-v_\Delta$ to guarantee the operation in the region of linear PWM modulation.

It is worth noting that there are 5th and 7th harmonic voltages resulted from the non-sinusoidal back-EMF or inverter non-linearity which turn into 6th harmonic voltages in the d_1q_1-d_2q_2-frame [41]. Assuming the 5th and 7th harmonics in the phase voltage are expressed as follows:

$$\begin{aligned} v_{5\&7\rm th} &= v_{5\rm th}+v_{7\rm th} \\ &= \begin{bmatrix} v_{a5\rm th}(\theta_e-0\theta_s)\\ v_{a5\rm th}(\theta_e-1\theta_s)\\ v_{a5\rm th}(\theta_e-4\theta_s)\\ v_{a5\rm th}(\theta_e-5\theta_s)\\ v_{a5\rm th}(\theta_e-8\theta_s)\\ v_{a5\rm th}(\theta_e-9\theta_s) \end{bmatrix} + \begin{bmatrix} v_{a7\rm th}(\theta_e-0\theta_s)\\ v_{a7\rm th}(\theta_e-1\theta_s)\\ v_{a7\rm th}(\theta_e-4\theta_s)\\ v_{a7\rm th}(\theta_e-5\theta_s)\\ v_{a7\rm th}(\theta_e-8\theta_s)\\ v_{a7\rm th}(\theta_e-9\theta_s) \end{bmatrix} \end{aligned} \tag{1}$$

where θ_e is the PM rotor electrical angle; and $v_{a5\rm th}(\theta_e)$ and $v_{a7\rm th}(\theta_e)$ are the 5th and 7th harmonics in phase-A, respectively. They can be expressed by the following equations, respectively, where k_{v5} and k_{v7} are the corresponding amplitudes, while θ_{v5} and θ_{v7} are the corresponding offset angle:

$$v_{a5\rm th}(\theta_e)=k_{v5}\cos\left(5\left(\theta_e+\pi/2\right)+\theta_{v5}\right) \tag{2}$$

$$v_{a7\rm th}(\theta_e)=k_{v7}\cos\left(7\left(\theta_e+\pi/2\right)+\theta_{v7}\right). \tag{3}$$

The 5th and 7th harmonic phase voltages are then converted to the 6th harmonics in the d_1q_1-d_2q_2-frame, which can be expressed as follows:

$$\begin{aligned} v_{d2\_6\rm th} =& -v_{d1\_6\rm th}=k_{v5}\sin(6\theta_e+\theta_{v5}) \\ &-k_{v7}\sin(6\theta_e+\theta_{v7}) \\ v_{q2\_6\rm th} =& -v_{q1\_6\rm th}=k_{v5}\cos(6\theta_e+\theta_{v5}) \\ &+k_{v7}\cos(6\theta_e+\theta_{v7}) \end{aligned} \tag{4}$$

where $v_{d1\_6\rm th}$ and $v_{q1\_6\rm th}$ are the 6th harmonic voltages in the d_1q_1-frame for phase ABC, $v_{d2\_6\rm th}$ and $v_{q2\_6\rm th}$ are 6th harmonic voltages in the d_2q_2-frame for phase XYZ, respectively. Therefore, the dq-axis voltages in phase-ABC and -XYZ

when accounting for the fundamental and 6th harmonics can be expressed as follows:

$$\begin{cases} v_{d1} = v_{d0} - (k_{v5}\sin(6\theta_e + \theta_{v5}) - k_{v7}\sin(6\theta_e + \theta_{v7})) \\ v_{q1} = v_{q0} - (k_{v5}\cos(6\theta_e + \theta_{v5}) + k_{v7}\cos(6\theta_e + \theta_{v7})) \end{cases} \tag{5}$$

$$\begin{cases} v_{d2} = v_{d0} + (k_{v5}\sin(6\theta_e + \theta_{v5}) - k_{v7}\sin(6\theta_e + \theta_{v7})) \\ v_{q2} = v_{q0} + (k_{v5}\cos(6\theta_e + \theta_{v5}) + k_{v7}\cos(6\theta_e + \theta_{v7})) \end{cases} \tag{6}$$

where v_{d0} and v_{q0} are dc components that are from the fundamental component in the phase voltage.

Assuming the output voltage is equal to the voltage reference, i.e., $v_{d1}^*{=}v_{d1}$, $v_{q1}^*{=}v_{q1}$, $v_{d2}^*{=}v_{d2}$, $v_{q2}^*{=}v_{q2}$, then the magnitude of output voltages v_{m1} and v_{m2} can be expressed as follows:

$$v_{m1} = \sqrt{v_{d1}^{*2} + v_{q1}^{*2}} v_{m2} \qquad = \sqrt{v_{d2}^{*2} + v_{q2}^{*2}}. \tag{7}$$

Substituting (5) and (6) into (7), it will be found that there is the 6th harmonic in the voltage magnitude feedback v_{m1} and v_{m2}, which will be validated in the experiment part Section IV-A. The 6th harmonics in v_{m1} and v_{m2} will propagate through the FW PI controllers and then result in 6th harmonics in the FW currents.

It is worth noting that the 6th harmonic currents in the d_1q_1-d_2q_2-frame cannot be suppressed effectively by the conventional PI controller. Therefore, a resonance control [47] with the center frequency of six times of fundament frequency is employed to suppress the 6th harmonic currents in the d_1q_1-d_2q_2-frame [41]. It should also be noted that since the FW currents of phase-ABC and -XYZ are from different FW controllers, they might be different due to the DT-PMSM asymmetry. Although the torque current i_q^* are the same, e.g., they are both from the speed controller, the i_{q1}^* and i_{q2}^* might be different due to the different FW currents and the constraints of the same current limit. Therefore, the currents of phase-ABC and phase-XYZ might be unbalanced.

III. Proposed FW Control Based on Vector Space Decomposition Control

According to the VSD theory for the dual three-phase system detailed in [3] and [41], the six-dimensional cartesian coordinate system in the *abc-xyz* frame can be decomposed into three orthogonal subspaces, i.e., $\alpha\beta$, z_1z_2, o_1o_2 subplanes. By a dedicated [T6] matrix transformation detailed in [3] and [41], different harmonics are projected to different subplanes, i.e., the fundamental and $(12k\pm1)$th, $k = 1, 2\ldots$ harmonics in the *abc-xyz* frame are projected to $\alpha\beta$ subplane; the $(6k\pm1)$th, $k = 1, 3, 5\ldots$ harmonics in the *abc-xyz* frame are projected to z_1z_2 subplane; the $(3k)$th, $k = 0, 1, 3, 5\ldots$ harmonics in the *abc-xyz* frame are projected to o_1o_2 subplane. Since the 5th and 7th harmonics are mapped to the z_1z_2 subplane rather than the $\alpha\beta$ subplane, this feature can be exploited for FW feedback control of DT-PMSM.

In the VSD control of DT-PMSM, the components in the *dq*-frame and *dqz*-frame can be derived by the following equations, respectively [41]:

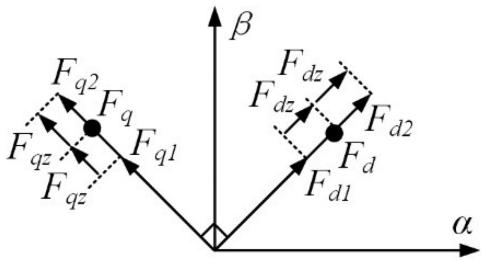

Fig. 3. Relationship between *d1q1-d2q2*-frame and *dq*-frame, *dqz*-frame.

$$\begin{bmatrix} F_d \\ F_q \end{bmatrix} = [T_{\text{park}}] \begin{bmatrix} F_\alpha \\ F_\beta \end{bmatrix} = \begin{bmatrix} \cos(\theta_e) & \sin(\theta_e) \\ -\sin(\theta_e) & \cos(\theta_e) \end{bmatrix} \begin{bmatrix} F_\alpha \\ F_\beta \end{bmatrix} \tag{8}$$

$$\begin{bmatrix} F_{dz} \\ F_{qz} \end{bmatrix} = [T_{dqz}] \begin{bmatrix} F_{z1} \\ F_{z2} \end{bmatrix} = \begin{bmatrix} -\cos(\theta_e) & \sin(\theta_e) \\ \sin(\theta_e) & \cos(\theta_e) \end{bmatrix} \begin{bmatrix} F_{z1} \\ F_{z2} \end{bmatrix}. \tag{9}$$

The VSD mathematical modeling of DT-PMSM is detailed in [38], where the voltage equations in the *dq*-frame and *dqz*-frame can be expressed as the following equations, respectively:

$$\begin{bmatrix} v_d \\ v_q \end{bmatrix} = \begin{bmatrix} R_s + L_d^{\text{equ}} s & 0 \\ 0 & R + L_q^{\text{equ}} s \end{bmatrix} \begin{bmatrix} i_d \\ i_q \end{bmatrix} + \omega \begin{bmatrix} -L_q^{\text{equ}} i_q \\ L_d^{\text{equ}} i_d + \psi_{fd} \end{bmatrix} \tag{10}$$

$$\begin{bmatrix} v_{dz} \\ v_{qz} \end{bmatrix} = \begin{bmatrix} R_s + L_{dz} s & 0 \\ 0 & R_s + L_{qz} s \end{bmatrix} \begin{bmatrix} i_{dz} \\ i_{qz} \end{bmatrix} + \omega \begin{bmatrix} -L_{qz} i_{qz} \\ L_{dz} i_{dz} \end{bmatrix} \tag{11}$$

where L_d^{equ} and L_q^{equ} are equivalent inductances in the *dq*-frame in $\alpha\beta$ subplane; L_{dz} and L_{qz} are equivalent inductances in the *dqz*-frame in z_1z_2 subplane; and ψ_{fd} is *d*-axis PM flux-linkage. As can be seen from (10), it has the same voltage equations as the single three-phase PMSM counterpart.

The relationship between the d_1q_1-d_2q_2-frame for the double single three-phase system and the *dq*-frame, *dqz*-frame based on VSD theory for the six-dimensional machine system can be illustrated in Fig. 3 [38], which can be expressed as follows:

$$\begin{aligned} F_{d2} &= F_d + F_{dz} \\ F_{d1} &= F_d - F_{dz} \end{aligned} \tag{12}$$

$$\begin{aligned} F_{q2} &= F_q + F_{qz} \\ F_{q1} &= F_q - F_{qz}. \end{aligned} \tag{13}$$

By combining (5), (6), (12), and (13), it can be derived that

$$\begin{bmatrix} v_{dz} \\ v_{qz} \end{bmatrix} = \begin{bmatrix} v_{d2\_6\text{th}} \\ v_{q2\_6\text{th}} \end{bmatrix} = - \begin{bmatrix} v_{d1\_6\text{th}} \\ v_{q1\_6\text{th}} \end{bmatrix}. \tag{14}$$

The abovementioned equation indicates that the 5th and 7th harmonic voltages are all mapped to the 6th harmonics in the *dqz*-frame. Therefore, the voltages in the *dq*-frame in the $\alpha\beta$ subplane are immune to the 6th harmonics.

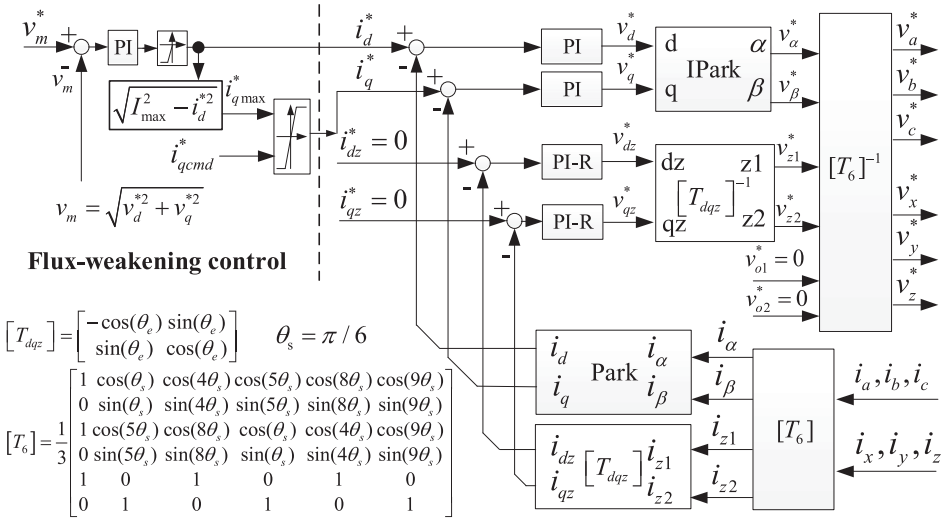

Fig. 4. Proposed FW control based on VSD control.

The magnitude of output voltage v_m in the *dq*-frame in the $\alpha\beta$ sub-plane can be expressed as follows:

$$v_m = \sqrt{v_d^{*2} + v_q^{*2}}. \tag{15}$$

As the fundamental components are projected to the $\alpha\beta$ subplane, the majority of the inverter output voltages are from the fundamental components in the $\alpha\beta$ subplane. Therefore, v_m can be employed for the voltage feedback in the FW control. As the v_m is 5th and 7th harmonics-free, it is beneficial for the generation of FW current reference.

The proposed FW control is illustrated in Fig. 4, which is based on VSD for DT-PMSM. By [T6], matrix transformation [41], the phase currents are converted to i_α, i_β in the $\alpha\beta$ subplane and i_{z1} , i_{z2} in the z_1z_2 subplane. The i_d an i_q are from conventional Park transformation applied to i_α and i_β. The i_{dz} and i_{qz} are from the $[T_{dqz}]$ transformation applied to i_{z1} and i_{z2}. The fundamental currents are regulated in the *dq*-frame in the $\alpha\beta$ subplane, while the harmonic currents are regulated in the *dqz*-frame in the z_1z_2 subplane [41]. As there are 5th and 7th harmonic voltages in the z_1z_2 subplane resulted from the nonsinusoidal back-EMF or inverter nonlinearity [41], and then they turn into the 6th harmonics in the *dqz*-frame in the z_1z_2 sub-plane, the resonance control with the center frequency of six times of fundament frequency is employed to suppress the sixth harmonic currents in the *dqz*-frame in the z_1z_2 subplane [41].

Besides, the common FW current is forwarded to both phase-ABC and phase-XYZ, where both channels share the same quadrature current reference i_q^* that comes from either the speed control or torque control, which depends on the application. Therefore, the currents of phase-ABC and -XYZ are naturally balanced in the proposed FW control based on the VSD control.

IV. Experiments

The test rig to evaluate the conventional FW control and the proposed FW control for DT-PMSM is constructed based on the TI DSP TMS320F28335 control system shown in Fig. 5. The dual inverter is employed to drive the machine, which has the same power topology, as shown in Fig. 1. The execution frequency of the current loop is the same as the PWM frequency of 10 kHz. Two independent SVPWM modulators are used for PWM generation for phase-ABC and -XYZ, respectively. The prototype DT-PMSM is coupled to another DT-PMSM used for load, which works in the torque control mode, while the prototype DT-PMSM works in the constant speed control mode. The parameters of the prototype DT-PMSM are listed in Table I.

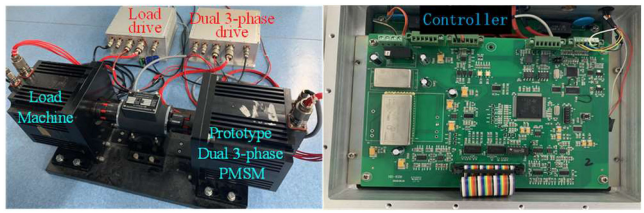

Fig. 5. Test rig for dual three-phase PMSM with phase Z open.

TABLE I
Parameters of Prototype Dual Three-Phase PMSM

Parameters	Value
Resistance (Ω)	0.08
Leakage inductance (mH)	0.864
d-axis self-inductance (mH)	2.82
q-axis self-inductance (mH)	5.00
Flux linkage (Wb)	0.0785
Pole pairs	5
Rated Power (W)	1200
Rated Current (A)	12
Rated torque (Nm)	19.1
Rated speed (rpm)	600
DC link voltage (V)	80

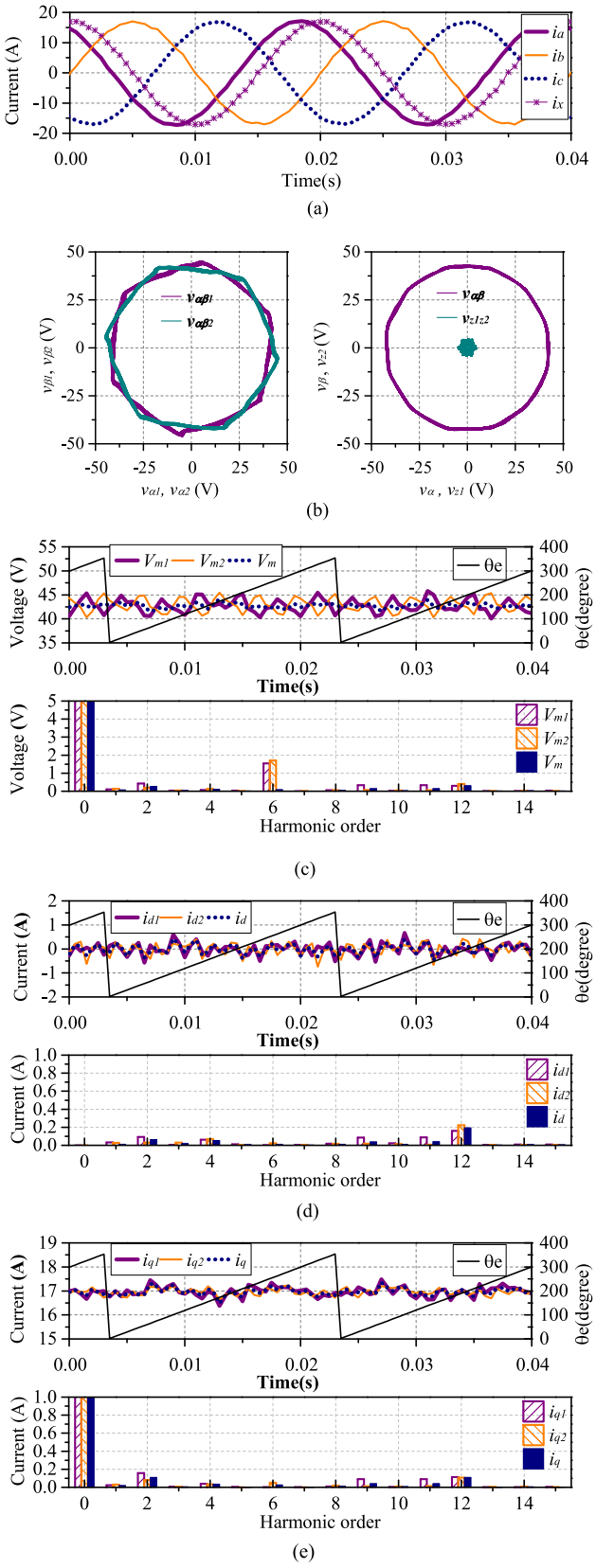

Fig. 6. Two-individual current control without FW (600 r/min constant speed control). (a) Phase currents. (b) Loci of $v_{\alpha\beta 1}$, $v_{\alpha\beta 2}$, $v_{\alpha\beta}$, and v_{z1z2}. (c) v_{m1}, v_{m2}, and v_m. (d) i_{d1}, i_{d2}, and i_d. (e) i_{q1}, i_{q2}, and i_q.

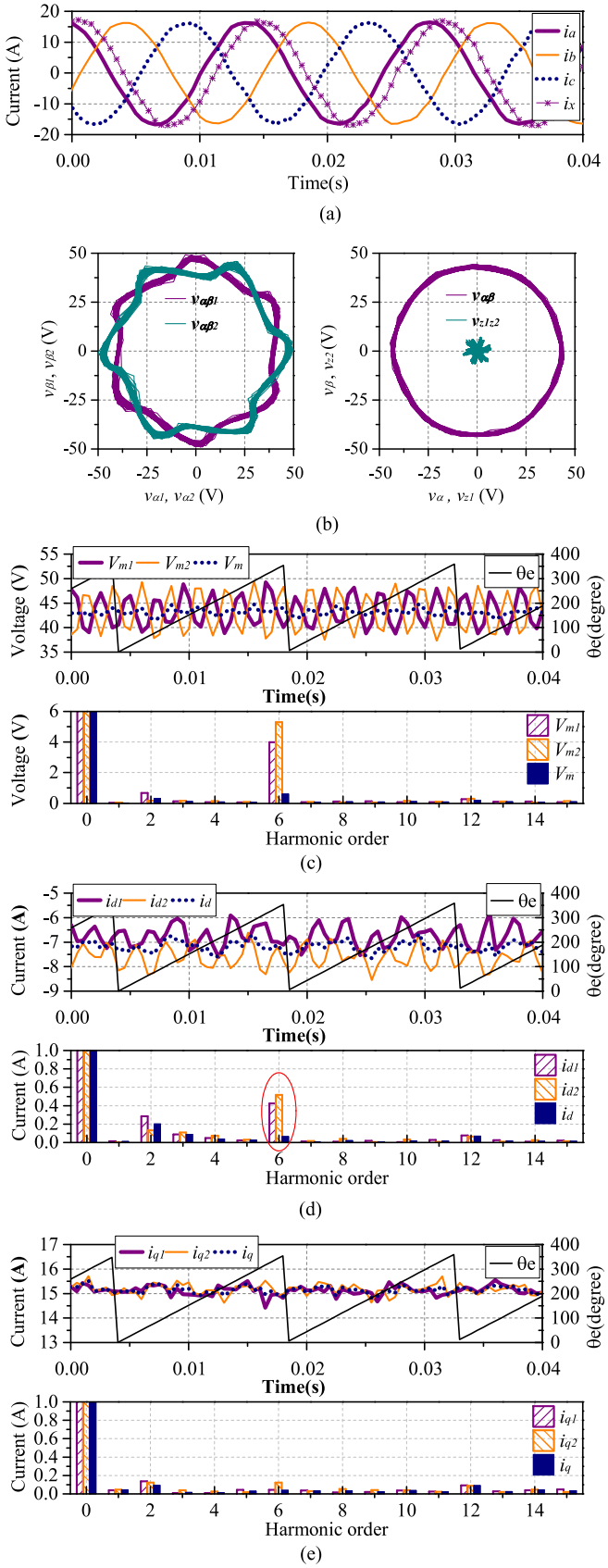

Fig. 7. Two-individual current control with FW (840 r/min, constant speed control). (a) Phase currents. (b) Loci of $v_{\alpha\beta 1}$, $v_{\alpha\beta 2}$, $v_{\alpha\beta}$, and v_{z1z2}. (c) v_{m1}, v_{m2}, and v_m. (d) i_{d1}, i_{d2}, and i_d. (e) i_{q1}, i_{q2}, and i_q.

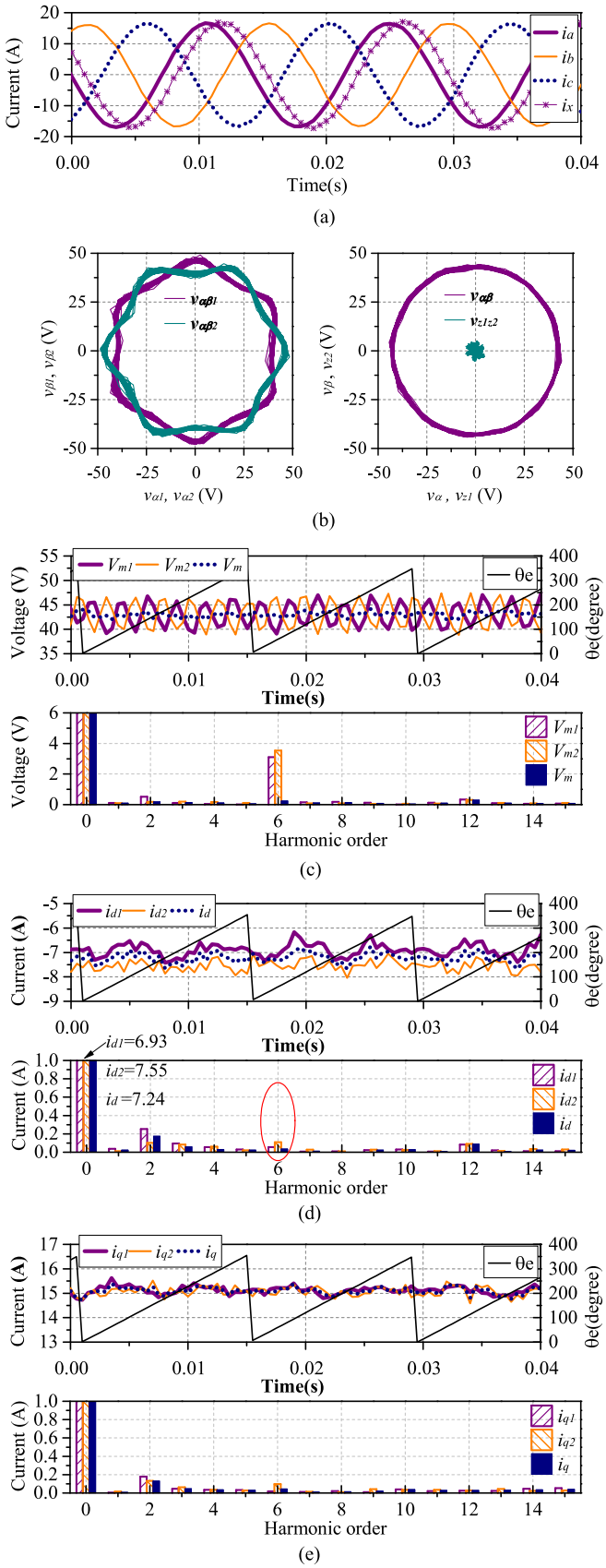

Fig. 8. Two-individual current control with FW and 2 ms LPF for i_d^* (840 r/min, constant speed control). (a) Phase currents. (b) Loci of $v_{\alpha\beta 1}$, $v_{\alpha\beta 2}$, $v_{\alpha\beta}$, and v_{z1z2}. (c) v_{m1}, v_{m2}, and v_m. (d) i_{d1}, i_{d2}, and i_d. (e) i_{q1}, i_{q2}, and i_q.

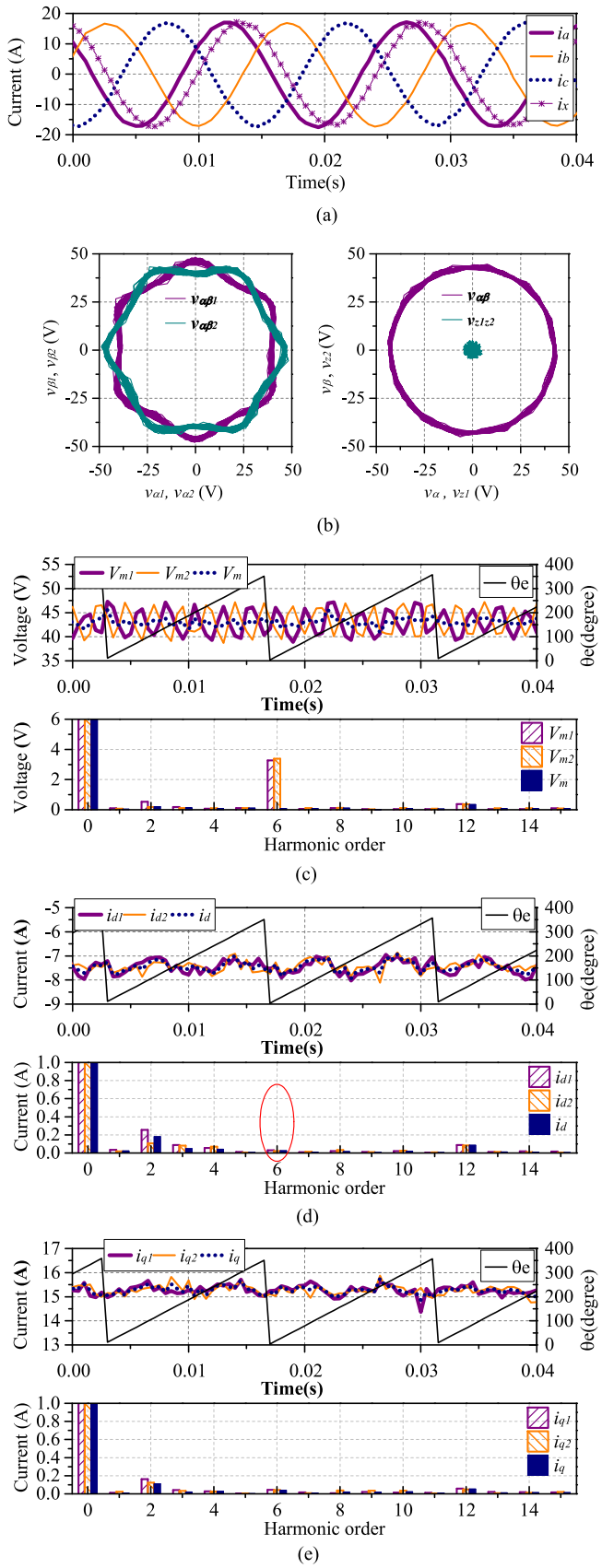

Fig. 9. Proposed FW control based on VSD (840 r/min, constant speed control). (a) Phase currents. (b) Loci of $v_{\alpha\beta 1}$, $v_{\alpha\beta 2}$, $v_{\alpha\beta}$, and v_{z1z2}. (c) v_{m1}, v_{m2}, and v_m. (d) i_{d1}, i_{d2}, and i_d. (e) i_{q1}, i_{q2}, and i_q.

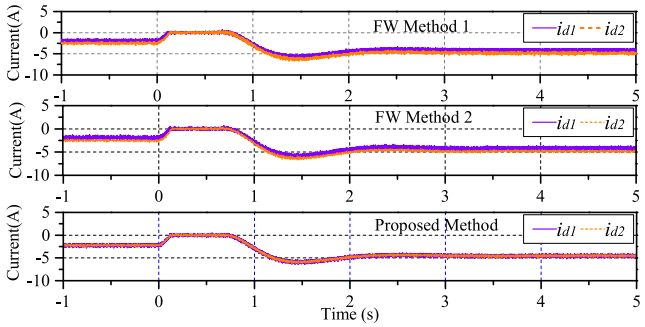

(a)

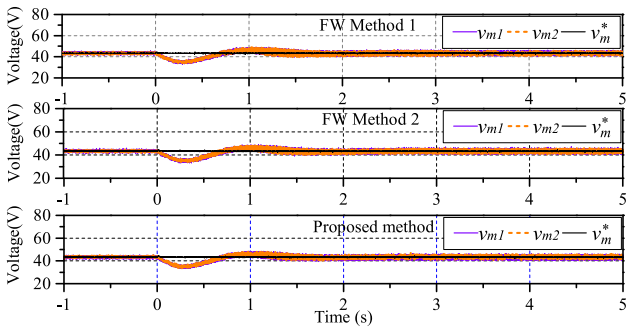

(b)

Fig. 10. Step response (FW Method-1: two-individual current control with FW, FW Method-2: two-individual current control with FW and 2 ms LPF for FW current reference, and the proposed FW control with VSD). (a) i_{d1} and i_{d2}. (b) v_{m1}, v_{m2} and v_m^*.

In this section, four experiments are conducted. The first is the two-individual current controls without FW control to demonstrate the phenomenon of the sixth harmonics in the output voltage in v_{m1} and v_{m2} , and explain why the output voltage magnitude v_m is chosen for voltage feedback in the FW control. The second is the conventional FW control based on two-individual current controls (FW Method-1) with v_{m1} and v_{m2} feedback with the main deficiencies of current unbalance and harmonics being presented. Then FW Method-1 is improved by adding a low-pass filter (LPF) before the generating FW current reference to suppress the harmonics in Fig. 2, which is named as FW Method-2. The third is the proposed FW with v_m feedback based on VSD control to exhibit its superiorities over the conventional FW control based on two-individual current controls in terms of reduction in current unbalance and harmonics. Finally, the dynamic performance of FW Method-1, FM Method-2, and the proposed FW control with VSD is evaluated.

A. Two-Individual Current Control Without FW Control

In this experiment, the two-individual current control in Fig. 2 is employed and the drive works in the constant speed mode, the i_q^* is from a speed loop and the speed reference is 600 r/min, and the corresponding fundamental frequency is 50 Hz. The dc bus voltage is set deliberately high so that the FW control modules in Fig. 2 are not activated. The i_d^* reference is set as zero. The loading machine works in the constant torque mode and the load is increased gradually until the prototype DT-PMSM current is approximately 12 A.

The experimental results are shown in Fig. 6. The phase currents are shown in Fig. 6(a), where the phase-X current $\boldsymbol{i_x}$ lags the phase-A current $\boldsymbol{i_a}$ by 30 °C. The rotor position is included in the top part of Fig. 6(c)–(e). The current profile and corresponding FFT analysis of *dq*-axis currents are shown in Fig. 6(d) and (e), respectively, showing that the sixth harmonics in $\boldsymbol{i_{d1}}$, $\boldsymbol{i_{d2}}$, $\boldsymbol{i_{q1}}$, and $\boldsymbol{i_{q2}}$ are well suppressed by the resonance controller.

The loci of output volage vector $\boldsymbol{v_{\alpha\beta 1}}$ $(\boldsymbol{v_{\alpha 1}} + \boldsymbol{jv_{\beta 1}})$ and $\boldsymbol{v_{\alpha\beta 2}}$ $(\boldsymbol{v_{\alpha 2}} + \boldsymbol{jv_{\beta 2}})$ for phase-ABC and -XYZ are shown in the left-hand side of Fig. 6(b). It is apparent that they are not a circle, which indicates that $\boldsymbol{v_{\alpha 1}}$, $\boldsymbol{v_{\beta 1}}$, $\boldsymbol{v_{\alpha 2}}$, and $\boldsymbol{v_{\beta 2}}$ are not sinusoidal. The loci of output voltage vectors in the $\boldsymbol{\alpha\beta}$ subplane $\boldsymbol{v_{\alpha\beta}}$ $(\boldsymbol{v_\alpha} + \boldsymbol{jv_\beta})$ and $\boldsymbol{z_1 z_2}$ subplane $\boldsymbol{v_{z1z2}}$ $(\boldsymbol{v_{z1}} + \boldsymbol{jv_{z2}})$ are shown in the right-hand side of Fig. 6(b). It is closer to a circle than the loci of $\boldsymbol{v_{\alpha\beta 1}}$ and $\boldsymbol{v_{\alpha\beta 2}}$, which means $\boldsymbol{v_\alpha}$ and $\boldsymbol{v_\beta}$ are much more sinusoidal than $\boldsymbol{v_{\alpha 1}}$, $\boldsymbol{v_{\beta 1}}$, $\boldsymbol{v_{\alpha 2}}$, and $\boldsymbol{v_{\beta 2}}$.

The magnitude of vectors $\boldsymbol{v_{\alpha\beta 1}}$, $\boldsymbol{v_{\alpha\beta 2}}$, and $\boldsymbol{v_{\alpha\beta}}$ changing with time and their corresponding FFT harmonic analysis are given in Fig. 6(c). From the harmonic analysis, it can be concluded that the major oscillations in $\boldsymbol{v_{m1}}$and $\boldsymbol{v_{m2}}$ are from 6th harmonic voltage, while the 6th harmonic voltage in $\boldsymbol{v_m}$ is insignificant. It also indicates that the 6th harmonics in $\boldsymbol{v_{m1}}$ and $\boldsymbol{v_{m2}}$ have the same amplitude but in the opposite phase; therefore, $\boldsymbol{v_m}$ has fewer oscillations than $\boldsymbol{v_{m1}}$ and $\boldsymbol{v_{m2}}$. Consequently, if $\boldsymbol{v_m}$ is employed as the voltage feedback in the FW control for DT-PMSM, it will be beneficial for the FW current reference without the 6th harmonic current.

B. Two-Individual Current Control With FW Control

In this experiment, the FW Method-1, i.e., the two-individual current control with FW shown in Fig. 2 is employed and the drive also works in the constant speed mode. The dc bus voltage is set as 82 V. To trig the FW control, the speed reference is set as 840 r/min and the corresponding fundamental frequency is 70 Hz. As the maximum linear output voltage with the SVPWM strategy is $82\ \text{V}/\sqrt{3} = 47.3\ \text{V}$, the voltage reference for FW is set as 42.3 V for enough voltage margin accounting for the harmonic voltage and inverter nonlinearity. The load is increased steadily until the rms current of the prototype machine increases up to 12 A. In this case, the FW currents for phase-ABC and -XYZ are not zero and the DT-PMSM works in the FW field.

The phase currents are shown in Fig. 7(a), the rotor position is included in the top part of Fig. 7(c)–(e), and the loci of output volage vector $\boldsymbol{v_{\alpha\beta 1}}$, $\boldsymbol{v_{\alpha\beta 2}}$, $\boldsymbol{v_{\alpha\beta}}$, and $\boldsymbol{v_{z1z2}}$ are shown in Fig. 7(b). The FW currents are shown in Fig. 7(d). The results show that the average FW current for phase-ABC and phase-XYZ are different, which means that currents of phase-ABC and phase-XYZ are unbalanced. The FFT analysis of i_{d1}, i_{d2}, and i_d shows that there are 2nd harmonic and 6th harmonic currents concurrently in i_{d1} and i_{d2}. The 2nd harmonic components in Fig. 7(d) are slightly higher than those in Fig. 6(d), which might be resulted from the asymmetry between phase-ABC and -XYZ. The 6th harmonic currents in i_{d1} and i_{d2} are resulted from the

6th harmonic voltages in output voltage feedback v_{m1} and v_{m2}, as shown in Fig. 7(c). There is negligible sixth harmonic in the i_d in Fig. 7(d), which is because the sixth harmonics in i_{d1} and i_{d2} have the same amplitude but in the opposite phase. However, it is worth highlighting that those harmonics will result in the deterioration of current total harmonic distortion (THD) and power loss in the system.

In the conventional FW control with two separate channels, the FW current reference comes directly from the FW PI control loop. To suppress the 6th harmonic component in the FW current, a LPF module can be added after the FW PI controller so that the 6th harmonic in the FW current reference can be suppressed. This method is named as FW Method-2 as mentioned earlier. In this experiment, a LPF with 2 ms time constant is applied to the FW controller output before the generation of i_{d1}^* and i_{d2}^*. The test condition is the same as that for FW Method-1. The experimental results are shown in Fig. 8, where the phase currents are shown in Fig. 8(a), the loci of $\boldsymbol{v_{\alpha\beta 1}}$, $\boldsymbol{v_{\alpha\beta 2}}$, $\boldsymbol{v_{\alpha\beta}}$, and $\boldsymbol{v_{z1z2}}$ are presented in Fig. 8(b), the output voltage feedback v_{m1} and v_{m2} are shown in Fig. 8(c), while the *dq*-axis currents are shown in Fig. 8(d) and (e), respectively. Fig. 8 is similar to Fig. 7 with the exception that the 6th harmonics in i_{d1} and i_{d2} are trivial. Although implementing a variable bandwidth filter requires more calculation power in the DSP, the experiment results show that it can be an effective way to suppress the 6th harmonics. However, the currents of phase-ABC and -XYZ are still unbalanced.

C. Proposed FW Control Based on VSD Control

In this experiment, the proposed FW control based on VSD control shown in Fig. 4 is employed and the prototype DT-PMSM works in the constant speed mode. To activate the FW control, the speed reference is set as 840 r/min and the corresponding fundamental frequency is 70 Hz. The dc bus voltage is set as 82 V and the voltage reference for FW is set as 42.3 V for enough voltage margin accounting for the harmonic voltage and inverter nonlinearity. The load is also increased steadily until the rms current of drive increases to 12 A. In this case, the DT-PMSM works in the FW field.

The loci of the output voltage vector $\boldsymbol{v_{\alpha\beta 1}}$, $\boldsymbol{v_{\alpha\beta 2}}$, $\boldsymbol{v_{\alpha\beta}}$, and $\boldsymbol{v_{z1z2}}$ are shown in Fig. 9(b). The magnitude of output voltage feedback v_{m1}, v_{m2}, and v_m are shown in Fig. 9(c). The results show that the 6th harmonic voltages are slightly lower than that in Fig. 7(c), which may be due to the lower 6th harmonics in i_{d1} and i_{d1}. Therefore, the reserved voltage margin v_Δ for linear PWM operation accounting for the harmonic voltage and inverter nonlinearity could be smaller, and then the output voltage reference v_m^* and power capability could be higher.

The phase currents are illustrated in Fig. 9(a). As can be seen, the phase currents are quite sinusoidal and the phase-X current i_x lags the phase-A current i_a by 30 °C. The rotor position is inlcuded in the top part of Fig. 9(c)–(e). The *d*-axis currents and corresponding FFT analysis are given in Fig. 9(d). Table II gives the harmonic components in i_{d1} andi_{d2} and their average value in Figs. 7(d), 8(d), and 9(d). Compared with those given in Fig. 7(d), there is negligible 6th harmonics in the i_{d1} and i_{d2}.

TABLE II
COMPARISON OF HARMONICS AND UNBALANCE

Magnitude	FW Method-1	FW Method-2	Proposal
6th harmonic in i_{d1}(A)	0.425	0.055	0.030
6th harmonic in i_{d2}(A)	0.517	0.108	0.021
Average i_{d1}(A)	-6.75	-6.73	-7.42
Average i_{d2}(A)	-7.57	-7.53	-7.42

Meanwhile, the average value of i_{d1} and i_{d2} are the same, which is much better than that in Fig. 7(d). The i_{q1} and i_{q2} are shown in Fig. 9(e), which are almost the same as well; therefore, the currents of phase-ABC and phase-XYZ are well balanced.

It is reported that the speed control performance could become worse due to the increased ripple of feedback voltage that is induced by the current reference ripple [48]; meanwhile, higher harmonic currents result in higher power loss and higher THD. Therefore, in terms of the current unbalance and the 6th harmonic current in i_{d1} and i_{d2}, the proposed FW control in Fig. 4 is superior to the conventional FW control extended for DT-PMSM in Fig. 2.

D. Comparison of Dynamic Performance

In this experiment, the load is stepped from 44% to 64% at the time of 0 s. The step response of FW Method-1, FW Method-2, and the proposed FW control with VSD control is shown in Fig. 10. The i_{d1} and i_{d2} response are illustrated in Fig. 10(a) while the output voltages are illustrated in Fig. 10(b). When the load is increased by 20% at 0 s, the speed drops instantaneously, and the output voltage v_{m1} and v_{m2} decreases as well; therefore, v_{m1} and v_{m2} will be lower than v_m^*. Consequently, FW current will arise and be limited to zero by a saturation module. As the speed ramps up, due to the constant speed control mode for the prototype DT-PMSM, the v_{m1} and v_{m2} rises up to v_m^* and then crosses over with overshoots. As the inputs of the FW current controllers become negative, the i_{d1} and i_{d2} decrease so as to lower the v_{m1} and v_{m2}. This process continues untill v_{m1} and v_{m2} agrees with the v_m^* in the steady state. As can be seen from Fig. 10, the dynamic performance of all the methods are almost the same, showing an excellent performance. However, it can be observed from Fig. 10(a) that average i_{d1} and i_{d2} in FW Method-1 and FW Method-2 are not equal in the steady state, which is the major deficiency of FW control based on the two-individual current control.

V. CONCLUSION

An FW control of DT-PMSM based on VSD control is proposed and compared with the conventional FW control for each set of single three-phase windings based on the two-individual current control in this article. In terms of reduction of the current unbalance and the harmonic current, the proposed approach is superior to the conventional FW control. In the proposed method, the magnitude of voltage in the $\alpha\beta$ subplane is employed for the voltage feedback. As the 5th and 7th harmonic voltage resulted from the nonsinusoidal back-EMF and inverter nonlinearity are mapped to the z_1z_2 subplane according to the

VSD theory, the voltage feedback in the FW control is 6th harmonic-free, so as the FW current. Meanwhile, because two sets of three-phase windings share the same FW current and torque current reference, their currents are naturally balanced. On the contrary, the FW currents for each set of three-phase windings in the conventional FW control are unbalanced, and they also have abundant 6th harmonic current if there is no LPF for the FW current reference. It is worth noting that the scenarios in this article are only investigated in the linear PWM region and the scenarios in the overmodulation region will be studied in the future.

REFERENCES

[1] L. Parsa, "On advantages of multi-phase machines," in *Proc. 31st Annu. Conf. IEEE Ind. Electron. Soc.*, 2005, pp. 1574–1579.

[2] M. A. Abbas, R. Christen, and T. M. Jahns, "Six-phase voltage source inverter driven induction motor," *IEEE Trans. Ind. Appl.*, vol. IA-20, no. 5, pp. 1251–1259, 1984.

[3] Y. F. Zhao and T. A. Lipo, "Space vector PWM control of dual three-phase induction machine using vector space decomposition," *IEEE Trans. Ind. Appl.*, vol. 31, no. 5, pp. 1100–1109, 1995.

[4] T. M. Jahns, "Improved reliability in solid-state AC drives by means of multiple independent phase drive units," *IEEE Trans. Ind. Appl.*, vol. IA-16, no. 3, pp. 321–331, 1980.

[5] K. Gopakumar, S. Sathiakumar, S. K. Biswas, and J. Vithayathil, "Modified current source inverter fed induction motor drive with reduced torque pulsations," *IEE Proc. B Elect. Power Appl.*, vol. 131, no. 4, pp. 159–164, 1984.

[6] G. K. Singh, K. Nam, and S. K. Lim, "A simple indirect field-oriented control scheme for multiphase induction machine," *IEEE Trans. Ind. Electron.*, vol. 52, no. 4, pp. 1177–1184, Aug. 2005.

[7] J. Karttunen, S. Kallio, P. Peltoniemi, P. Silventoinen, and O. Pyrhonen, "Dual three-phase permanent magnet synchronous machine supplied by two independent voltage source inverters," in *Proc. Int. Symp. Power Electron., Electr. Drives, Autom. Motion*, 2012, pp. 741–747.

[8] E. Levi, R. Bojoi, F. Profumo, H. A. Toliyat, and S. Williamson, "Multiphase induction motor drives—A technology status review," *IET Electr. Power Appl.*, vol. 1, no. 4, pp. 489–516, 2007.

[9] E. Levi, "Multiphase electric machines for variable-speed applications," *IEEE Trans. Ind. Electron.*, vol. 55, no. 5, pp. 1893–1909, May 2008.

[10] L. de Lillo, P. Wheeler, L. Empringham, and C. Gerada, "Multiphase power converter drive for fault-tolerant machine development in aerospace applications," *IEEE Trans. Ind. Electron.*, vol. 57, no. 2, pp. 575–583, Feb. 2010.

[11] W. Cao, B. C. Mecrow, G. J. Atkinson, J. W. Bennett, and D. J. Atkinson, "Overview of electric motor technologies used for more electric aircraft (MEA)," *IEEE Trans. Ind. Electron.*, vol. 59, no. 9, pp. 3523–3531, Sep. 2012.

[12] H. Amimeur, D. Aouzellag, R. Abdessemed, and K. Ghedamsi, "Sliding mode control of a dual-stator induction generator for wind energy conversion systems," *Int. J. Electr. Power Engery Syst.*, vol. 42, no. 1, pp. 60–70, 2012.

[13] D. Yazdani, S. Ali Khajehoddin, A. Bakhshai, and G. Joos, "Full utilization of the inverter in split-phase drives by means of a dual three-phase space vector classification algorithm," *IEEE Trans. Ind. Electron.*, vol. 56, no. 1, pp. 120–129, Feb. 2009.

[14] R. F. Schiferl and T. A. Lipo, "Power capability of salient pole permanent magnet synchronous motors in variable speed drive applications," *IEEE Trans. Ind. Appl.*, vol. 26, no. 1, pp. 115–123, Jan./Feb. 1990.

[15] W. L. Soong and T. J. E. Miller, "Field-weakening performance of brushless synchronous AC motor drives," *IEE Proc.–Elect. Power Appl.*, vol. 141, no. 6, pp. 331–340, 1994.

[16] C. Wang, Z. Q. Zhu, and H. Zhan, "Adaptive voltage feedback controllers on non-salient permanent magnet synchronous machine," *IEEE Trans. Ind. Appl.*, vol. 56, no. 2, pp. 1529–1542, Mar./Apr. 2019.

[17] S. Morimoto, Y. Takeda, T. Hirasa, and K. Taniguchi, "Expansion of operating limits for permanent magnet motor by current vector control considering inverter capacity," *IEEE Trans. Ind. Appl.*, vol. 26, no. 5, pp. 866–871, Sep./Oct. 1990.

[18] B. Cheng and T. R. Tesch, "Torque feedforward control technique for permanent-magnet synchronous motors," *IEEE Trans. Ind. Electron.*, vol. 57, no. 3, pp. 969–974, Mar. 2010.

[19] S. Morimoto, M. Sanada, and Y. Takeda, "Effects and compensation of magnetic saturation in flux-weakening controlled permanent magnet synchronous motor drives," *IEEE Trans. Ind. Appl.*, vol. 30, no. 6, pp. 1632–1637, Nov./Dec. 1994.

[20] R. Dhaouadi and N. Mohan, "Analysis of current-regulated voltage-source inverters for permanent magnet synchronous motor drives in normal and extended speed ranges," *IEEE Trans. Energy Convers.*, vol. 5, no. 1, pp. 137–144, Mar. 1990.

[21] M. Tursini, E. Chiricozzi, and R. Petrella, "Feedforward flux-weakening control of surface-mounted permanent-magnet synchronous motors accounting for resistive voltage drop," *IEEE Trans. Ind. Electron.*, vol. 57, no. 1, pp. 440–448, Jan. 2010.

[22] H. W. de Kock, A. J. Rix, and M. J. Kamper, "Optimal torque control of synchronous machines based on finite-element analysis," *IEEE Trans. Ind. Electron.*, vol. 57, no. 1, pp. 413–419, Jan. 2010.

[23] S. D. Sudhoff, K. A. Corzine, and H. J. Hegner, "A flux-weakening strategy for current-regulated surface-mounted permanent-magnet machine drives," *IEEE Trans. Energy Convers.*, vol. 10, no. 3, pp. 431–437, Sep. 1995.

[24] J.-M. Kim and S.-K. Sul, "Speed control of interior permanent magnet synchronous motor drive for the flux weakening operation," *IEEE Trans. Ind. Appl.*, vol. 33, no. 1, pp. 43–48, Jan./Feb. 1997.

[25] N. Bianchi, S. Bolognani, and M. Zigliotto, "High-performance PM synchronous motor drive for an electrical scooter," *IEEE Trans. Ind. Appl.*, vol. 37, no. 5, pp. 1348–1355, Sep./Oct. 2001.

[26] L. Harnefors, K. Pietilainen, and L. Gertmar, "Torque-maximizing field-weakening control: Design, analysis, and parameter selection," *IEEE Trans. Ind. Electron.*, vol. 48, no. 1, pp. 161–168, Feb. 2001.

[27] S. Bolognani, S. Calligaro, and R. Petrella, "Adaptive flux-weakening controller for interior permanent magnet synchronous motor drives," *IEEE J. Emerg. Sel. Top. Power Electron.*, vol. 2, no. 2, pp. 236–248, Jun. 2014.

[28] N. Bedetti, S. Calligaro, and R. Petrella, "Analytical design and autotuning of adaptive flux-weakening voltage regulation loop in IPMSM drives with accurate torque regulation," *IEEE Trans. Ind. Appl.*, vol. 56, no. 1, pp. 301–313, Jan./Feb. 2020.

[29] T. Deng, Z. Su, J. Li, P. Tang, X. Chen, and P. Liu, "Advanced angle field weakening control strategy of permanent magnet synchronous motor," *IEEE Trans. Veh. Technol.*, vol. 68, no. 4, pp. 3424–3435, Apr. 2019.

[30] Z. Dong, Y. Yu, W. Li, B. Wang, and D. Xu, "Flux-weakening control for induction motor in voltage extension region: Torque analysis and dynamic performance improvement," *IEEE Trans. Ind. Electron.*, vol. 65, no. 5, pp. 3740–3751, May 2018.

[31] H. Liu, Z. Q. Zhu, E. Mohamed, Y. Fu, and X. Qi, "Flux-weakening control of nonsalient pole PMSM having large winding inductance, accounting for resistive voltage drop and inverter nonlinearities," *IEEE Trans. Power Electron.*, vol. 27, no. 2, pp. 942–952, Feb. 2012.

[32] Y. Kwon, S. Kim, and S. Sul, "Voltage feedback current control scheme for improved transient performance of permanent magnet synchronous machine drives," *IEEE Trans. Ind. Electron.*, vol. 59, no. 9, pp. 3373–3382, Sep. 2012.

[33] B. Stumberger, G. Stumberger, D. Dolinar, A. Hamler, and M. Trlep, "Evaluation of saturation and cross-magnetization effects in interior permanent-magnet synchronous motor," *IEEE Trans. Ind. Appl.*, vol. 39, no. 5, pp. 1264–1271, Sep./Oct. 2003.

[34] S. Bolognani, L. Peretti, M. Zigliotto, and E. Bertotto, "Commissioning of electromechanical conversion models for high dynamic PMSM drives," *IEEE Trans. Ind. Electron.*, vol. 57, no. 3, pp. 986–993, Mar. 2010.

[35] T. Kwon, G. Choi, M. Kwak, and S. Sul, "Novel flux-weakening control of an IPMSM for quasi-six-step operation," *IEEE Trans. Ind. Appl.*, vol. 44, no. 6, pp. 1722–1731, Nov./Dec. 2008.

[36] B. Bon-Ho, N. Patel, S. Schulz, and S. Seung-Ki, "New field weakening technique for high saliency interior permanent magnet motor," in *Proc. 38th IAS Annu. Meeting Conf. Rec. Ind. Appl. Conf.*, 2003, vol. 2, pp. 898–905.

[37] L. Ping-Yi and L. Yen-Shin, "Voltage control technique for the extension of dc-link voltage utilization of finite-speed SPMSM drives," *IEEE Trans. Ind. Electron.*, vol. 59, no. 9, pp. 3392–3402, Sep. 2012.

[38] Y. Hu, Z. Q. Zhu, and M. Odavic, "Comparison of two-individual current control and vector space decomposition control for dual three-phase PMSM," *IEEE Trans. Ind. Appl.*, vol. 53, no. 5, pp. 4483–4492, Sep./Oct. 2017.

[39] R. Bojoi, M. Lazzari, F. Profumo, and A. Tenconi, "Digital field-oriented control for dual three-phase induction motor drives," *IEEE Trans. Ind. Appl.*, vol. 39, no. 3, pp. 752–760, May/Jun. 2003.
[40] R. Bojoi, F. Profumo, and A. Tenconi, "Digital synchronous frame current regulation for dual three-phase induction motor drives," in *Proc. IEEE 34th Annu. Power Electron. Spec. Conf.*, 2003, vol. 3, pp. 1475–1480.
[41] Y. Hu, Z.-Q. Zhu, and K. Liu, "Current control for dual three-phase permanent magnet synchronous motors accounting for current unbalance and harmonics," *IEEE J. Emerg. Sel. Topics Power Electron.*, vol. 2, no. 2, pp. 272–284, Jun. 2014.
[42] J. Karttunen, S. Kallio, P. Peltoniemi, P. Silventoinen, and O. Pyrhonen, "Decoupled vector control scheme for dual three-phase permanent magnet synchronous machines," *IEEE Trans. Ind. Electron.*, vol. 61, no. 5, pp. 2185–2196, May 2014.
[43] L. Yongjae and H. Jung-Ik, "High efficiency dual inverter drives for a PMSM considering field weakening region," in *Proc. 7th Int. Power Electron. Motion Control Conf.*, 2012, pp. 1009–1014.
[44] S. Liu and C. Liu, "Flux weakening control for dual three-phase PMSM," in *Proc. Asia-Pacific Magn. Recording Conf.*, 2018, pp. 1–2.
[45] L. Yan and D. Chengfei, "Flux weakening control technology of multiphase PMSG for aeronautical high voltage dc power supply system," in *Proc. 22nd Int. Conf. Elect. Mach. Syst.*, 2019, pp. 1–5.
[46] S. Bozhko, S. S. Yeoh, F. Gao, and C. Hill, "Aircraft starter-generator system based on permanent-magnet machine fed by active front-end rectifier," in *Proc. 40th Annu. Conf. IEEE Ind. Electron. Soc.*, 2014, pp. 2958–2964.
[47] D. N. Zmood and D. G. Holmes, "Stationary frame current regulation of PWM inverters with zero steady-state error," *IEEE Trans. Power Electron.*, vol. 18, no. 3, pp. 814–822, May 2003.
[48] C. Wang and Z. Q. Zhu, "Fuzzy logic speed control of permanent magnet synchronous machine and feedback voltage ripple reduction in flux-weakening operation region," *IEEE Trans. Ind. Appl.*, vol. 56, no. 2, pp. 1505–1517, Mar./ Apr. 2020.

Yashan Hu received the B.Eng. and M.Sc. degrees from the Northwestern Polytechnical University, Xi'an, China, in 2002 and 2005, respectively, and the Ph.D. degree from the University of Sheffield, Sheffield, U.K, in 2016, all in electronic and electrical engineering.

From 2016 to 2018, he was with Siemens Wind Power A/S, Denmark, as an Advanced Research Engineer. Since 2018, he has been an Associate Professor with the College of Electrical and Information Engineering, Hunan University, Changsha, China. His current research interests include electrical machine control and drives for applications ranging from automotive to renewable energy.

Yonggang Li was born in 1994. He received the B.E. degree from the School of Electrical and Electronic Engineering, Shanghai Institute of Technology, Shanghai, China, in 2015, and the M.E. degrees from the China University of Mining and Technology, Xuzhou, China, in 2019. He is currently working toward the Ph.D. degree with the College of Electrical and Information Engineering, Hunan University, Changsha, China.

His research interests include analysis and control of multiphase machine driving system, direct-drive and doubly fed wind power converter control.

Xiandong Ma received the B.Eng. degree in electrical engineering from Jiangsu University, Zhenjiang, China, in 1986, the M.Sc. degree in power systems and automation from China State Grid Electric Power Research Institute, Nanjing, China, in 1989, and the Ph.D. degree in partial discharge-based high-voltage condition monitoring from Glasgow Caledonian University, Glasgow, U.K, in 2003.

He is a Senior Lecturer with the Department of Engineering, Lancaster University, Lancashire, U.K. His research interests include intelligent condition monitoring and fault diagnosis of the renewable energy systems particularly with wind power generation, distributed energy generation and smart grids, advanced signal processing, and instrumentation. He has authored and coauthored more than 120 papers in the leading international journals, book chapters, and international conferences, and holds patents.

Dr. Ma is also an Associate Editor of the *IEEE Systems Journal* and the *International Journal of Automation and Computing*. He is a Chartered Engineer (C.Eng.) and a fellow of the Institution of Engineering and Technology (FIET).

Xuefei Li received the B.Eng. degree in electronic and electrical engineering from the Northwestern Polytechnical University, Xi'an, China, in 2003.

Since 2018, she has been a Research Assistant with the College of Electrical and Information Engineering, Hunan University, Changsha, China. Her current research interests include power electronic systems and control, electrical machine control and drives.

Shoudao Huang (Senior Member, IEEE) was born in Hunan, China, in 1962. He received the B.S. and Ph.D. degrees in electrical engineering from the College of Electrical and Information Engineering, Hunan University, Changsha, China, in 1983 and 2005, respectively.

He is currently a Full Professor with the College of Electrical and Information Engineering, Hunan University. His research interests include machine design and control, power electronic systems and control, and wind energy conversion systems.